Low-momentum direct-photon measurement in Cu + Cu collisions at $\sqrt{s_{NN}} = 200$ GeV

A. Adare,[12] S. Afanasiev,[30] C. Aidala,[13,45] N. N. Ajitanand,[64,*] Y. Akiba,[58,59,†] H. Al-Bataineh,[52] J. Alexander,[64] M. Alfred,[23] K. Aoki,[32,35,58] L. Aphecetche,[66] R. Armendariz,[52] S. H. Aronson,[6] J. Asai,[59] E. T. Atomssa,[36] R. Averbeck,[65] T. C. Awes,[54] B. Azmoun,[6] V. Babintsev,[24] A. Bagoly,[17] G. Baksay,[19] L. Baksay,[19] A. Baldisseri,[15] K. N. Barish,[7] P. D. Barnes,[39,*] B. Bassalleck,[51] S. Bathe,[4,7,59] S. Batsouli,[54] V. Baublis,[57] A. Bazilevsky,[6] S. Belikov,[6,*] R. Belmont,[12] R. Bennett,[65] A. Berdnikov,[61] Y. Berdnikov,[61] A. A. Bickley,[12] M. Boer,[39] J. G. Boissevain,[39] J. S. Bok,[52] H. Borel,[15] K. Boyle,[59,65] M. L. Brooks,[39] J. Bryslawskyj,[7] H. Buesching,[6] V. Bumazhnov,[24] G. Bunce,[6,59] S. Butsyk,[39,65] S. Campbell,[13,65] V. Canoa Roman,[65] B. S. Chang,[74] J.-L. Charvet,[15] S. Chernichenko,[24] C. Y. Chi,[13] J. Chiba,[32] M. Chiu,[6,25] I. J. Choi,[25,74] T. Chujo,[69,70] P. Chung,[64] A. Churyn,[24] V. Cianciolo,[54] C. R. Cleven,[21] B. A. Cole,[13] M. P. Comets,[55] M. Connors,[21,59] P. Constantin,[39] M. Csanád,[17] T. Csörgő,[18,73] T. Dahms,[65] T. W. Danley,[53] K. Das,[20] G. David,[6,65] M. B. Deaton,[1] K. Dehmelt,[19,65] H. Delagrange,[66,*] A. Denisov,[24] D. d'Enterria,[13] A. Deshpande,[59,65] E. J. Desmond,[6] O. Dietzsch,[62] A. Dion,[65] J. H. Do,[74] M. Donadelli,[62] O. Drapier,[36] A. Drees,[65] A. K. Dubey,[72] J. M. Durham,[39] A. Durum,[24] V. Dzhordzhadze,[7] Y. V. Efremenko,[54] J. Egdemir,[65] F. Ellinghaus,[12] W. S. Emam,[7] A. Enokizono,[38,58,60] H. En'yo,[58,59] S. Esumi,[69] K. O. Eyser,[6,7] W. Fan,[65] N. Feege,[65] D. E. Fields,[51,59] M. Finger,[8,30] M. Finger, Jr.,[8,30] F. Fleuret,[36] S. L. Fokin,[34] Z. Fraenkel,[72,*] J. E. Frantz,[53,65] A. Franz,[6] A. D. Frawley,[20] K. Fujiwara,[58] Y. Fukao,[35,58] T. Fusayasu,[48] S. Gadrat,[40] P. Gallus,[14] P. Garg,[3,65] I. Garishvili,[38,67] H. Ge,[65] A. Glenn,[12,38] H. Gong,[65] M. Gonin,[36] J. Gosset,[15] Y. Goto,[58,59] R. Granier de Cassagnac,[36] N. Grau,[2,28] S. V. Greene,[70] M. Grosse Perdekamp,[25,59] T. Gunji,[11] H.-Å. Gustafsson,[41,*] T. Hachiya,[22,49,59] A. Hadj Henni,[66] C. Haegemann,[51] J. S. Haggerty,[6] H. Hamagaki,[11] R. Han,[56] H. Harada,[22] E. P. Hartouni,[38] K. Haruna,[22] S. Hasegawa,[29] T. O. S. Haseler,[21] E. Haslum,[41] R. Hayano,[11] X. He,[21] M. Heffner,[38] T. K. Hemmick,[65] T. Hester,[7] H. Hiejima,[25] J. C. Hill,[28] K. Hill,[12] R. Hobbs,[51] A. Hodges,[21] M. Hohlmann,[19] W. Holzmann,[64] K. Homma,[22] B. Hong,[33] T. Horaguchi,[58,68] D. Hornback,[67] T. Hoshino,[22] N. Hotvedt,[28] J. Huang,[6] T. Ichihara,[58,59] H. Iinuma,[35,58] K. Imai,[29,35,58] M. Inaba,[69] Y. Inoue,[58,60] D. Isenhower,[1] L. Isenhower,[1] M. Ishihara,[58] T. Isobe,[11] M. Issah,[64] A. Isupov,[30] D. Ivanishchev,[57] B. V. Jacak,[65] Z. Ji,[65] J. Jia,[6,13,64] J. Jin,[13] O. Jinnouchi,[59] B. M. Johnson,[6,21] K. S. Joo,[47] D. Jouan,[55] F. Kajihara,[11] S. Kametani,[11,71] N. Kamihara,[58] J. Kamin,[65] M. Kaneta,[59] J. H. Kang,[74] H. Kanou,[58,68] D. Kawall,[44,59] A. V. Kazantsev,[34] V. Khachatryan,[65] A. Khanzadeev,[57] J. Kikuchi,[71] D. H. Kim,[47] D. J. Kim,[31,74] E. Kim,[63] E.-J. Kim,[9] M. Kim,[63] D. Kincses,[17] E. Kinney,[12] Á. Kiss,[17] E. Kistenev,[6] A. Kiyomichi,[58] J. Klay,[38] C. Klein-Boesing,[46] L. Kochenda,[57] V. Kochetkov,[24] B. Komkov,[57] M. Konno,[69] D. Kotchetkov,[7,53] D. Kotov,[57,61] A. Kozlov,[72] A. Král,[14] A. Kravitz,[13] J. Kubart,[8,27] G. J. Kunde,[39] B. Kurgyis,[17] N. Kurihara,[11] K. Kurita,[58,60] M. J. Kweon,[33] Y. Kwon,[67,74] G. S. Kyle,[52] R. Lacey,[64] Y. S. Lai,[13] J. G. Lajoie,[28] A. Lebedev,[28] D. M. Lee,[39] M. K. Lee,[74] S. H. Lee,[28] T. Lee,[63] M. J. Leitch,[39] M. A. L. Leite,[62] B. Lenzi,[62] Y. H. Leung,[65] N. A. Lewis,[45] X. Li,[10] X. Li,[39] S. H. Lim,[39,74] T. Liška,[14] A. Litvinenko,[30] M. X. Liu,[39] S. Lökös,[17] B. Love,[70] D. Lynch,[6] C. F. Maguire,[70] T. Majoros,[16] Y. I. Makdisi,[5] A. Malakhov,[30] M. D. Malik,[51] V. I. Manko,[34] Y. Mao,[56,58] L. Mašek,[8,27] H. Masui,[69] F. Matathias,[13] M. McCumber,[39,65] P. L. McGaughey,[39] D. McGlinchey,[12,39] Y. Miake,[69] A. C. Mignerey,[43] D. E. Mihalik,[65] P. Mikeš,[8,27] K. Miki,[69] T. E. Miller,[70] A. Milov,[65,72] S. Mioduszewski,[6] M. Mishra,[3] J. T. Mitchell,[6] M. Mitrovski,[64] G. Mitsuka,[32,59] T. Moon,[74] A. Morreale,[7] D. P. Morrison,[6] S. I. Morrow,[70] T. V. Moukhanova,[34] D. Mukhopadhyay,[70] J. Murata,[58,60] S. Nagamiya,[32,58] K. Nagashima,[22] Y. Nagata,[69] J. L. Nagle,[12] M. Naglis,[72] I. Nakagawa,[58,59] Y. Nakamiya,[22] T. Nakamura,[22] K. Nakano,[58,68] J. Newby,[38] M. Nguyen,[65] B. E. Norman,[39] R. Nouicer,[6,59] T. Novák,[18] N. Novitzky,[65] A. S. Nyanin,[34] E. O'Brien,[6] S. X. Oda,[11] C. A. Ogilvie,[28] H. Ohnishi,[58] M. Oka,[69] K. Okada,[59] O. O. Omiwade,[1] J. D. Orjuela Koop,[12] J. D. Osborn,[45] A. Oskarsson,[41] M. Ouchida,[22] K. Ozawa,[11,32,69] R. Pak,[6] D. Pal,[70] A. P. T. Palounek,[39] V. Pantuev,[26,65] V. Papavassiliou,[52] J. Park,[63] S. Park,[58,63,65] W. J. Park,[33] S. F. Pate,[52] M. Patel,[28] H. Pei,[28] J.-C. Peng,[25] W. Peng,[70] H. Pereira,[15] D. V. Perepelitsa,[12] V. Peresedov,[30] D. Yu. Peressounko,[34] C. E. PerezLara,[65] C. Pinkenburg,[6] M. L. Purschke,[6] A. K. Purwar,[39] H. Qu,[21] P. V. Radzevich,[61] J. Rak,[31,51] A. Rakotozafindrabe,[36] I. Ravinovich,[72] K. F. Read,[54,67] S. Rembeczki,[19] M. Reuter,[65] K. Reygers,[46] V. Riabov,[50,57] Y. Riabov,[57,61] D. Richford,[4] T. Rinn,[28] G. Roche,[40,*] A. Romana,[36,*] M. Rosati,[28] S. S. E. Rosendahl,[41] P. Rosnet,[40] Z. Rowan,[4] P. Rukoyatkin,[30] J. Runchey,[28] V. L. Rykov,[58] B. Sahlmueller,[46,65] N. Saito,[32,35,58,59] T. Sakaguchi,[6] S. Sakai,[69] H. Sakata,[22] H. Sako,[29] V. Samsonov,[50,57] M. Sarsour,[21] S. Sato,[29,32] S. Sawada,[32] B. K. Schmoll,[67] J. Seele,[12] R. Seidl,[25,58,59] V. Semenov,[24] R. Seto,[7] D. Sharma,[65,72] I. Shein,[24] A. Shevel,[57,64] T.-A. Shibata,[58,68] K. Shigaki,[22] M. Shimomura,[28,49,69] K. Shoji,[35,58] A. Sickles,[25,65] C. L. Silva,[39,62] D. Silvermyr,[41,54] C. Silvestre,[15] K. S. Sim,[33] C. P. Singh,[3] V. Singh,[3] M. J. Skoby,[45] S. Skutnik,[28] M. Slunečka,[8,30] A. Soldatov,[24] R. A. Soltz,[38] W. E. Sondheim,[39] S. P. Sorensen,[67] I. V. Sourikova,[6] F. Staley,[15] P. W. Stankus,[54] E. Stenlund,[41] M. Stepanov,[52,*] A. Ster,[73] S. P. Stoll,[6] T. Sugitate,[22] C. Suire,[55] Z. Sun,[16] J. Sziklai,[73] T. Tabaru,[59] S. Takagi,[69] E. M. Takagui,[62] A. Taketani,[58,59] Y. Tanaka,[48] K. Tanida,[29,58,59,63] M. J. Tannenbaum,[6] A. Taranenko,[50,64] P. Tarján,[16] T. L. Thomas,[51] R. Tieulent,[42] M. Togawa,[35,58] A. Toia,[65] J. Tojo,[58] L. Tomášek,[27] H. Torii,[58] R. S. Towell,[1] V.-N. Tram,[36] I. Tserruya,[72] Y. Tsuchimoto,[22] Y. Ueda,[22] B. Ujvari,[16] C. Vale,[28] H. Valle,[70] H. W. van Hecke,[39] J. Velkovska,[70] R. Vértesi,[16,73] A. A. Vinogradov,[34] M. Virius,[14] V. Vrba,[14,27] E. Vznuzdaev,[57] M. Wagner,[35,58] D. Walker,[65] X. R. Wang,[52,59] D. Watanabe,[22] Y. Watanabe,[58,59] F. Wei,[28,52] J. Wessels,[46] S. N. White,[6] D. Winter,[13] C. P. Wong,[21] C. L. Woody,[6] M. Wysocki,[12,54] W. Xie,[59] C. Xu,[52] Q. Xu,[70] Y. L. Yamaguchi,[59,65,71]

A. Yanovich,[24] Z. Yasin,[7] J. Ying,[21] S. Yokkaichi,[58,59] J. H. Yoo,[33] G. R. Young,[54] I. Younus,[37,51] H. Yu,[52] I. E. Yushmanov,[34] W. A. Zajc,[13] O. Zaudtke,[46] C. Zhang,[54] S. Zharko,[61] S. Zhou,[10] J. Zimamyi,[73,*] L. Zolin,[30] and L. Zou[7]
(PHENIX Collaboration)

[1]*Abilene Christian University, Abilene, Texas 79699, USA*
[2]*Department of Physics, Augustana University, Sioux Falls, South Dakota 57197, USA*
[3]*Department of Physics, Banaras Hindu University, Varanasi 221005, India*
[4]*Baruch College, City University of New York, New York, New York, 10010 USA*
[5]*Collider-Accelerator Department, Brookhaven National Laboratory, Upton, New York 11973-5000, USA*
[6]*Physics Department, Brookhaven National Laboratory, Upton, New York 11973-5000, USA*
[7]*University of California-Riverside, Riverside, California 92521, USA*
[8]*Charles University, Ovocný trh 5, Praha 1, 116 36, Prague, Czech Republic*
[9]*Chonbuk National University, Jeonju, 561-756, Korea*
[10]*Science and Technology on Nuclear Data Laboratory, China Institute of Atomic Energy, Beijing 102413, People's Republic of China*
[11]*Center for Nuclear Study, Graduate School of Science, University of Tokyo, 7-3-1 Hongo, Bunkyo, Tokyo 113-0033, Japan*
[12]*University of Colorado, Boulder, Colorado 80309, USA*
[13]*Columbia University, New York, New York 10027 and Nevis Laboratories, Irvington, New York 10533, USA*
[14]*Czech Technical University, Zikova 4, 166 36 Prague 6, Czech Republic*
[15]*Dapnia, CEA Saclay, F-91191, Gif-sur-Yvette, France*
[16]*Debrecen University, H-4010 Debrecen, Egyetem tér 1, Hungary*
[17]*ELTE, Eötvös Loránd University, H-1117 Budapest, Pázmány P. s. 1/A, Hungary*
[18]*Eszterházy Károly University, Károly Róbert Campus, H-3200 Gyöngyös, Mátrai út 36, Hungary*
[19]*Florida Institute of Technology, Melbourne, Florida 32901, USA*
[20]*Florida State University, Tallahassee, Florida 32306, USA*
[21]*Georgia State University, Atlanta, Georgia 30303, USA*
[22]*Hiroshima University, Kagamiyama, Higashi-Hiroshima 739-8526, Japan*
[23]*Department of Physics and Astronomy, Howard University, Washington, DC 20059, USA*
[24]*IHEP Protvino, State Research Center of Russian Federation, Institute for High Energy Physics, Protvino, 142281, Russia*
[25]*University of Illinois at Urbana-Champaign, Urbana, Illinois 61801, USA*
[26]*Institute for Nuclear Research of the Russian Academy of Sciences, prospekt 60-letiya Oktyabrya 7a, Moscow 117312, Russia*
[27]*Institute of Physics, Academy of Sciences of the Czech Republic, Na Slovance 2, 182 21 Prague 8, Czech Republic*
[28]*Iowa State University, Ames, Iowa 50011, USA*
[29]*Advanced Science Research Center, Japan Atomic Energy Agency, 2-4 Shirakata Shirane, Tokai-mura, Naka-gun, Ibaraki-ken 319-1195, Japan*
[30]*Joint Institute for Nuclear Research, 141980 Dubna, Moscow Region, Russia*
[31]*Helsinki Institute of Physics and University of Jyväskylä, P.O.Box 35, FI-40014 Jyväskylä, Finland*
[32]*KEK, High Energy Accelerator Research Organization, Tsukuba, Ibaraki 305-0801, Japan*
[33]*Korea University, Seoul, 136-701, Korea*
[34]*National Research Center "Kurchatov Institute", Moscow, 123098 Russia*
[35]*Kyoto University, Kyoto 606-8502, Japan*
[36]*Laboratoire Leprince-Ringuet, Ecole Polytechnique, CNRS-IN2P3, Route de Saclay, F-91128, Palaiseau, France*
[37]*Physics Department, Lahore University of Management Sciences, Lahore 54792, Pakistan*
[38]*Lawrence Livermore National Laboratory, Livermore, California 94550, USA*
[39]*Los Alamos National Laboratory, Los Alamos, New Mexico 87545, USA*
[40]*LPC, Université Blaise Pascal, CNRS-IN2P3, Clermont-Fd, 63177 Aubiere Cedex, France*
[41]*Department of Physics, Lund University, Box 118, SE-221 00 Lund, Sweden*
[42]*IPNL, CNRS/IN2P3, Univ Lyon, UniversitÃ© Lyon 1, F-69622, Villeurbanne, France*
[43]*University of Maryland, College Park, Maryland 20742, USA*
[44]*Department of Physics, University of Massachusetts, Amherst, Massachusetts 01003-9337, USA*
[45]*Department of Physics, University of Michigan, Ann Arbor, Michigan 48109-1040, USA*
[46]*Institut für Kernphysik, University of Münster, D-48149 Münster, Germany*
[47]*Myongji University, Yongin, Kyonggido 449-728, Korea*
[48]*Nagasaki Institute of Applied Science, Nagasaki-shi, Nagasaki 851-0193, Japan*
[49]*Nara Women's University, Kita-uoya Nishi-machi Nara 630-8506, Japan*
[50]*National Research Nuclear University, MEPhI, Moscow Engineering Physics Institute, Moscow, 115409, Russia*
[51]*University of New Mexico, Albuquerque, New Mexico 87131, USA*
[52]*New Mexico State University, Las Cruces, New Mexico 88003, USA*
[53]*Department of Physics and Astronomy, Ohio University, Athens, Ohio 45701, USA*
[54]*Oak Ridge National Laboratory, Oak Ridge, Tennessee 37831, USA*

[55]*IPN-Orsay, Univ. Paris-Sud, CNRS/IN2P3, Université Paris-Saclay, BP1, F-91406, Orsay, France*
[56]*Peking University, Beijing 100871, People's Republic of China*
[57]*PNPI, Petersburg Nuclear Physics Institute, Gatchina, Leningrad region, 188300, Russia*
[58]*RIKEN Nishina Center for Accelerator-Based Science, Wako, Saitama 351-0198, Japan*
[59]*RIKEN BNL Research Center, Brookhaven National Laboratory, Upton, New York 11973-5000, USA*
[60]*Physics Department, Rikkyo University, 3-34-1 Nishi-Ikebukuro, Toshima, Tokyo 171-8501, Japan*
[61]*Saint Petersburg State Polytechnic University, St. Petersburg, 195251 Russia*
[62]*Universidade de São Paulo, Instituto de Física, Caixa Postal 66318, São Paulo CEP05315-970, Brazil*
[63]*Department of Physics and Astronomy, Seoul National University, Seoul 151-742, Korea*
[64]*Chemistry Department, Stony Brook University, SUNY, Stony Brook, New York 11794-3400, USA*
[65]*Department of Physics and Astronomy, Stony Brook University, SUNY, Stony Brook, New York 11794-3800, USA*
[66]*SUBATECH (Ecole des Mines de Nantes, CNRS-IN2P3, Université de Nantes) BP 20722-44307, Nantes, France*
[67]*University of Tennessee, Knoxville, Tennessee 37996, USA*
[68]*Department of Physics, Tokyo Institute of Technology, Oh-okayama, Meguro, Tokyo 152-8551, Japan*
[69]*Tomonaga Center for the History of the Universe, University of Tsukuba, Tsukuba, Ibaraki 305, Japan*
[70]*Vanderbilt University, Nashville, Tennessee 37235, USA*
[71]*Waseda University, Advanced Research Institute for Science and Engineering, 17 Kikui-cho, Shinjuku-ku, Tokyo 162-0044, Japan*
[72]*Weizmann Institute, Rehovot 76100, Israel*
[73]*Institute for Particle and Nuclear Physics, Wigner Research Centre for Physics, Hungarian Academy of Sciences (Wigner RCP, RMKI) H-1525 Budapest 114, POBox 49, Budapest, Hungary*
[74]*Yonsei University, IPAP, Seoul 120-749, Korea*

(Received 13 May 2018; published 15 November 2018)

We measured direct photons for $p_T < 5$ GeV/c in minimum bias and 0%–40% most-central events at midrapidity for Cu+Cu collisions at $\sqrt{s_{NN}} = 200$ GeV. The e^+e^- contribution from quasireal direct virtual photons has been determined as an excess over the known hadronic contributions in the e^+e^- mass distribution. A clear enhancement of photons over the binary scaled $p+p$ fit is observed for $p_T < 4$ GeV/c in Cu+Cu data. The p_T spectra are consistent with the Au+Au data covering a similar number of participants. The inverse slopes of the exponential fits to the excess after subtraction of the $p+p$ baseline are $285 \pm 53(\text{stat}) \pm 57(\text{syst})$ MeV/c and $333 \pm 72(\text{stat}) \pm 45(\text{syst})$ MeV/c for minimum bias and 0%–40% most-central events, respectively. The rapidity density, dN/dy, of photons demonstrates the same power law as a function of $dN_{\text{ch}}/d\eta$ observed in Au+Au at the same collision energy.

DOI: 10.1103/PhysRevC.98.054902

I. INTRODUCTION

Direct photons are excellent probes for understanding the time evolution of the hot and dense matter created in ultrarelativistic heavy-ion collisions [1,2]. Direct photons are produced throughout the collision and carry information about the medium at the time when the photons were emitted, because the only interaction is electromagnetic [3]. Direct photons are produced via interactions at partonic and hadronic levels in either initial hard scatterings of the collision or thermal radiation from the medium and, by definition, do not originate from hadron decays [4]. In particular, thermal photons, which contribute dominantly at low momentum [5], are one of the most important probes because they allow us direct access to the thermodynamic properties of the created medium. However, photons from hadron decays account for a large fraction in the inclusive photon yield, typically more than 80% for heavy-ion collisions. The large number of decay photons makes the measurement challenging.

Two analysis methods, the virtual photon method [6] and the external conversion method [7], have been established to measure direct photons at low p_T ($p_T < 5$ GeV/c). Low-p_T direct-photon measurements have been made in PHENIX and STAR experiments at the Relativistic Heavy Ion Collider (RHIC) for not only in Au+Au collisions [6–8] but also in $p+p$ and d+Au [9] collisions. The virtual photon method makes it possible to measure direct photons even if the signal to background (S/B) is only a few percent, as in $p+p$ and d+Au collisions, while in Au+Au collisions the S/B reaches 15%. The $p+p$ measurement allows us to determine the hard photon yield from initial hard scatterings. No significant modification of the p_T distribution of direct photons due to cold nuclear effects is seen in the d+Au data. Finally, an enhanced yield of low-p_T direct photons, which

*Deceased.
†akiba@rcf.rhic.bnl.gov

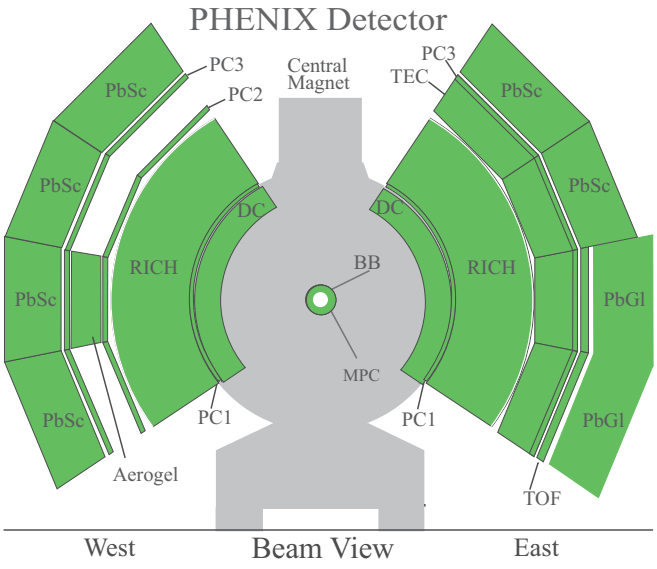

FIG. 1. The beam view of the PHENIX detector configuration in 2005.

is unexplainable by hard photon production and cold nuclear matter effects, has been discovered in Au+Au collisions in central and semicentral events at $\sqrt{s_{NN}} = 200$ GeV [6,7].

The ALICE experiment at the Large Hadron Collider (LHC) has also succeeded in measuring the low-p_T direct photons with the external conversion method in Pb + Pb collisions at $\sqrt{s_{NN}} = 2.76$ TeV [10] and observed a larger yield and a higher inverse slope of the spectrum than at RHIC, implying that a larger and hotter thermalized medium is produced at the LHC energy. Further understanding of the thermal properties of the created hot medium can be realized through the systematic study of low-p_T direct photon production within a wide range of system size and collision energy.

In this paper, we present the measurement of low-p_T direct photons in Cu+Cu collisions at $\sqrt{s_{NN}} = 200$ GeV with the virtual photon method. This measurement may provide additional information on the system size dependence of low-p_T direct-photon production. This paper focuses on two centrality classes, minimum bias (MB) and 0%–40% most-central collisions, for which the number of participants, $N_{\rm part}$, is similar to peripheral Au+Au ($N_{\rm part} = 34.6 \pm 1.2$ [11] and 66.4 ± 2.5 [12]).

II. THE PHENIX DETECTOR

The two PHENIX central arm spectrometers in conjunction with the beam-beam counters (BBCs) are used for this measurement. Figure 1 shows the beam view of the PHENIX detector configuration for the 2005 run. The BBCs, with rapidity coverage $3.1 < |\eta| < 3.9$, are located at ± 144 cm away from the nominal interaction point. They measure charged particles that are used to determine the z-vertex position, the centrality, and the event plane. They provide the MB event trigger with a trigger efficiency of 94%. The two central arms cover $|\eta| < 0.35$ and an azimuthal angle range of $\pi/2$ per arm. Each arm is instrumented with a drift chamber (DC) and pad chambers (PCs) that determine the trajectories and, together with a magnetic field, measure the momenta of charged particles. The material in front of the DC is minimal, 0.39% of a radiation length, to allow for a good momentum resolution of $\delta p/p = 1\% \oplus 1.1\% \times p$ [GeV/c] above 0.2 GeV/c [13], and to minimize the amount of photon conversions. Eight separate sectors of electromagnetic calorimeters (EMCals) composed of two lead-glass (PbGl) calorimeters in the bottom sectors of the east arm and six lead-scintillator (PbSc) calorimeters for the remainder, provide an electromagnetic shower energy measurement with resolution $\Delta E/E$ of $2.1\% \oplus 8.1\%/\sqrt{E}$ for PbSc and of $0.8\% \oplus 5.9\%/\sqrt{E}$ for PbGl (E in GeV) [13]. Requiring energy-momentum matching with an associated hit in the Ring Imaging Čerenkov counter (RICH) provides a hadron rejection factor of better than 10^4, thus providing good electron identification. The mass resolution for e^+e^- pairs is determined with a Monte Carlo simulation which is tuned to match the shape of the reconstructed e^+e^- mass distribution in the data below 90 MeV/c^2 [14], where e^+e^- pairs from π^0 Dalitz decays are dominant. The calculated e^+e^- mass resolution is $\sigma_{ee} = 3.1$ MeV/c^2 for $1 < p_T < 2$ GeV/c, and it increases by about 1 MeV/c^2 per GeV/c as p_T increases.

III. ANALYSIS

Low-p_T direct photons, measured by using the virtual photon method, are the subject of this analysis. Any production process of direct photons has a higher-order process producing a quasireal virtual photon, which then produces a low-mass, high-p_T e^+e^- pair. The relation between the photon emission (dN_γ) and associate electron pair rates (dN_{ee}) is expressed as

$$\frac{d^2N_{ee}}{dm_{ee}} = \frac{2\alpha}{3\pi}\frac{1}{m_{ee}}\sqrt{1-\frac{4m_e^2}{m_{ee}^2}}\left(1+\frac{2m_e^2}{m_{ee}^2}\right)SdN_\gamma, \quad (1)$$

where α, m_e, m_{ee} are the fine-structure constant and masses for the electron and the electron pair, respectively. S is introduced to factor out the difference between real and virtual photon emission. It is a process-dependent factor because it accounts for the effects of form factors, phase space, and spectral functions [15]. For direct virtual photons satisfying $p_T \gg m_{ee}$, S is almost unity, while it drops to 0 as m_{ee} approaches the parent hadron mass in case of hadron decays. As a result, S introduces a shape difference of the e^+e^- mass distributions for virtual photons and hadron decays. The key idea of this measurement is to utilize this shape difference. Therefore, the contribution of the e^+e^- pairs internally converted via virtual photons is determined as an excess yield over the known hadronic contributions in the mass region above the π^0 mass, typically $0.1 < m_{ee} < 0.3$ GeV/c^2, by a template fit. The direct-photon fraction at $m_{ee} = 0$ is then obtained by extrapolation of the template fit result. Finally, the obtained direct-photon fraction can be converted to the real direct photon yield by using the measured inclusive photon yield. A detailed description of the virtual photon method can be found in Ref. [15].

This measurement is based on a MB sample of 4.95×10^8 200 GeV Cu+Cu collisions with z vertex within 25 cm of

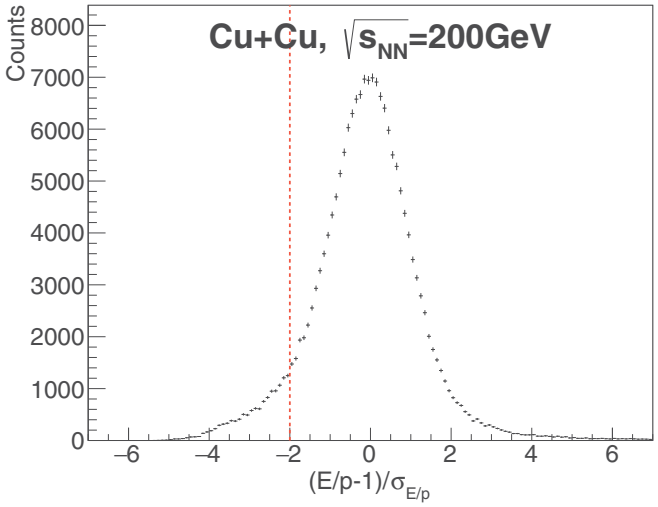

FIG. 2. The E/p distribution for electrons from pairs with p_T of $1-2\,\mathrm{GeV}/c$ after applying all cuts for electron identification except for E/p.

the nominal interaction point collected in 2005, equivalent to $0.44\,\mathrm{nb}^{-1}$. All electrons with $p_T^e > 0.3\,\mathrm{GeV}/c$ are paired in each event. These e^+e^- pairs are required to have $p_T > 1\,\mathrm{GeV}/c$.

Figure 2 shows the E/p distribution for electrons from pairs with p_T of $1-2\,\mathrm{GeV}/c$, where E is measured with the EMCal, and p from the track radius in the magnetic field. All electron identification cuts except for E/p are applied for this figure. Because hadrons do not deposit their full energy in the EMCal, hadron contamination produces a tail in the negative region. This plot indicates the excellent purity of the electron sample. All electron candidates are required to have $(E/p-1)/\sigma_{E/p} > -2$, resulting in negligible hadron contamination.

Undesired pairs from several background sources contaminate the foreground pair distribution. The first source is fake pairs due to accidentally overlapping hits in various detectors. RICH ring-sharing and cluster overlaps in the PCs are the main sources for these fake pairs. They can be removed by geometric analysis cuts [15,16]. The RICH ring-sharing cut requires separation of ring centers for the two electrons of a pair to be greater than 25 cm, which is larger than the expected maximum diameter of a RICH ring, ∼16.8 cm. Tracks are also required to be separated by $\Delta z > 0.5\,\mathrm{cm}$ and $\Delta\phi > 0.02$ rad to remove overlap in the PCs.

The second background source is photon conversions in the detector material. These can be eliminated because the PHENIX tracking algorithm, which assumes all tracks come from the collision vertex, introduces an artificial opening angle of the conversion pairs with the decay plane perpendicular to the magnetic field.

A. Background evaluation

After removing the detector-oriented fake pairs and conversions, the foreground distributions for unlike-sign (FG_{+-}) and like-sign pairs (FG_{--}, FG_{++}) can be expressed as

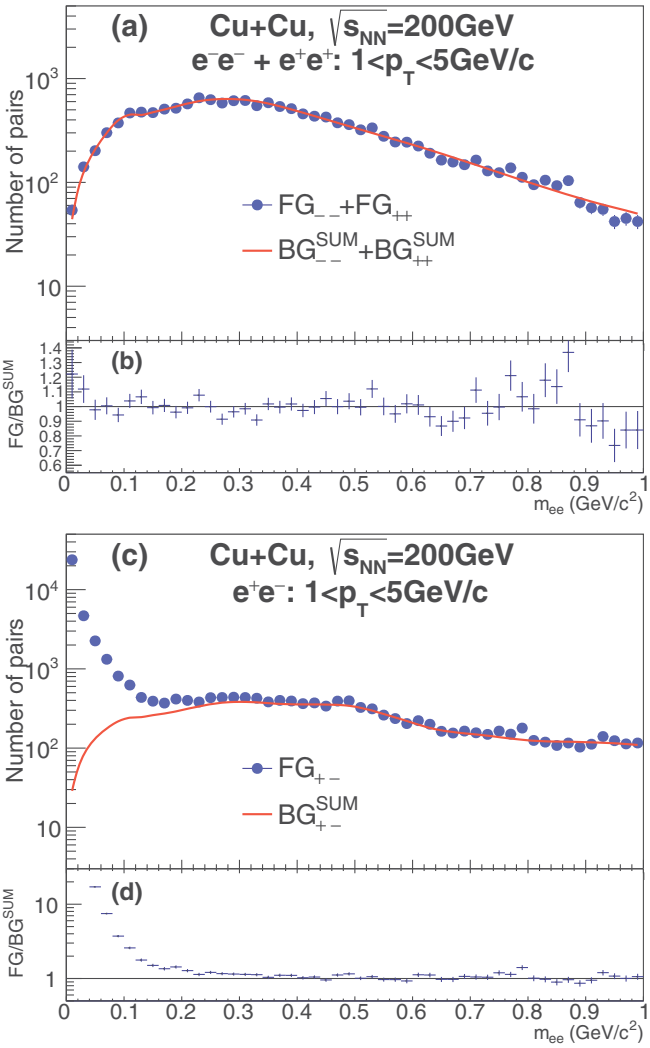

FIG. 3. (a) Like-sign and (c) unlike-sign mass distributions of the data together with $\mathrm{BG}^{\mathrm{SUM}}$ normalized by the $\mathrm{BG}^{\mathrm{SUM}}$ fit for $1 < p_T < 5\,\mathrm{GeV}/c$. (b), (d) Ratios of data over $\mathrm{BG}^{\mathrm{SUM}}$.

$$\mathrm{FG}_{--} = \mathrm{BG}^{\mathrm{CM}}_{--} + \mathrm{BG}^{\mathrm{JT}}_{--} + \mathrm{BG}^{\mathrm{XC}}_{--} = \mathrm{BG}^{\mathrm{SUM}}_{--}, \quad (2)$$

$$\mathrm{FG}_{++} = \mathrm{BG}^{\mathrm{CM}}_{++} + \mathrm{BG}^{\mathrm{JT}}_{++} + \mathrm{BG}^{\mathrm{XC}}_{++} = \mathrm{BG}^{\mathrm{SUM}}_{++}, \quad (3)$$

$$\mathrm{FG}_{+-} = S + \mathrm{BG}^{\mathrm{SUM}}_{+-} + \mathrm{HD}_{+-}. \quad (4)$$

Here FG refers to the data and BG refers to backgrounds whose shapes are calculated as described below, but whose normalization comes from a fit to the data (FG). S refers to the direct virtual photon signal and HD refers to correlated pairs from known hadron decays. It is notable that the like-sign pair distributions are composed of only random combinations ($\mathrm{BG}^{\mathrm{CM}}$), jet-induced correlations ($\mathrm{BG}^{\mathrm{JT}}$), and correlated fake pairs from double Dalitz decays of the π^0, η ($\mathrm{BG}^{\mathrm{XC}}$). The sum of these backgrounds is referred to as $\mathrm{BG}^{\mathrm{SUM}}$ in this paper. Once compositions of these background contributions are known in the like-sign combination sample, the unlike-sign combination background, $\mathrm{BG}^{\mathrm{SUM}}_{+-}$, can be determined within the same analysis framework.

1. Combinatorial background

The combinatorial background can be reproduced by the event mixing technique with event classification with respect to z-vertex position, event plane, and centrality. However, the modulation of the mass distribution by the elliptic flow, which is apparent in the real events, is not fully introduced in event mixing because of the limited reaction plane resolution. Thus, pairs in the mixed events are weighted by a factor based on the measured azimuthal anisotropy of single electrons [16] for given reaction plane classes. The weighting factor w, depending on the opening angle of a pair, is calculated as

$$w(\Delta\phi) = 1 + 2v_2^a v_2^b \cos 2(\Delta\phi), \tag{5}$$

where $\Delta\phi$, $v_2^{a,b}$ are the pair opening angle and azimuthal anisotropy of each electron in a pair, respectively. The flow modulation makes at most a few percent difference in the mass shape.

2. Jet-induced correlation

Jet-induced correlations are pairs in which each electron is from a different parent, but both parents are from the same jet or back-to-back jets. Such events are simulated by PYTHIA8 [17,18] with CTEQ5L [19] parton distribution functions. The PYTHIA8-generated events are passed through a GEANT3-based [20] simulation of the PHENIX detector in which all detector effects such as the acceptance and efficiencies are taken into account. Uncorrelated combinations are evaluated by the event mixing technique within the simulated events. It is found that the shape of the like-sign mass distribution for the uncorrelated combinations is consistent with that for the foreground combinations in $0.6 < m_{ee} < 1.1$ GeV/c^2. Here, the true and other correlated pairs are removed from the foreground distribution before the comparison. Normalization of the uncorrelated combinations in a specific region of a pair opening angle, where opening angle distributions for correlated and uncorrelated pairs are consistent, gives a consistent result. A detailed description can be found in Ref. [16]. Finally the jet-induced correlations are obtained by removing uncorrelated combinations from the simulated mass distribution.

3. Correlated Dalitz and double Dalitz cross pairs

The other non-negligible source of correlated background is cross combinations from decays having two electron pairs in the final state, i.e., π^0 and η double Dalitz decays and Dalitz decays with a subsequent photon conversion. These cross combinations are localized at the very low mass region below the π^0 and η masses. The mass distributions of these cross combinations from π^0 and η are calculated by using the aforementioned GEANT3 simulation with the π^0 and η distributions measured by PHENIX.

4. Background normalization by $\mathrm{BG}^{\mathrm{SUM}}$ *fit*

The calculated BG_{--} and BG_{++} distributions are the ingredients for a fit to FG_{--} and FG_{++}, which then yields the contribution of each component to the background, $\mathrm{BG}^{\mathrm{SUM}}$. Pairs from the same jet and back-to-back jets are separately included in the fit because they are influenced differently by jet quenching. The $\mathrm{BG}^{\mathrm{SUM}}$ fit to FG_{--} and FG_{++} works very well. Figure 3 shows the like-sign and unlike-sign mass distributions of the data together with $\mathrm{BG}^{\mathrm{SUM}}$ normalized by the $\mathrm{BG}^{\mathrm{SUM}}$ fit for $1 < p_T < 5$ GeV/c where the virtual photon analysis is performed. The normalized $\mathrm{BG}^{\mathrm{SUM}}$ is in good agreement with the data for like-sign pairs. The contribution of the physically correlated pairs [$S + \mathrm{HD}_{+-}$ in Eq. (4)] is significant in the foreground unlike-sign pair mass distribution below 0.3 GeV/c^2.

A cross-check with the like-sign subtraction method [21] is done to demonstrate that the $\mathrm{BG}^{\mathrm{SUM}}_{+-}$ properly accounts for all backgrounds. To infer the background in unlike-sign distributions, a correction must be made to account for the relative acceptance difference between like- and unlike-sign pairs. Thus, the acceptance-corrected like-sign pairs should

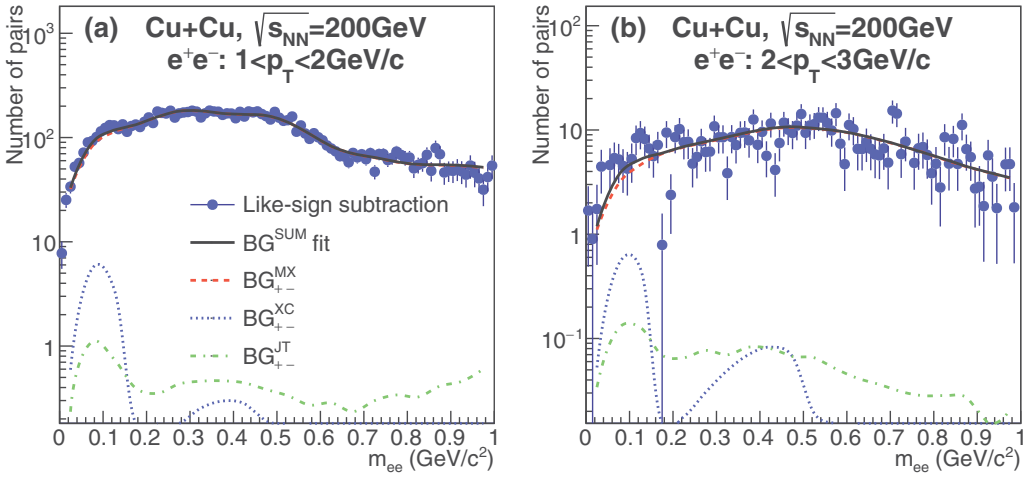

FIG. 4. Background pair distributions of e^+e^- determined by like-sign subtraction method, $\alpha_{\mathrm{acc}}(\mathrm{FG}_{--} + \mathrm{FG}_{++})$ (circle symbols), and $\mathrm{BG}^{\mathrm{SUM}}$ fit method (solid curves) for (a) $p_T = 1$–2 GeV/c and (b) 2–3 GeV/c. The resulting contributions to $\mathrm{BG}^{\mathrm{SUM}}_{+-}$ are also shown by dashed, dotted, and dashed-dotted curves (see text and legend).

TABLE I. Hagedorn fit parameters for the π^0 distribution in 0%–40% centrality and MB in Cu+Cu collisions.

Fit parameter	0%–40%	MB
A [mb GeV$^{-2}c^3$]	$(3.5 \pm 2.8) \times 10^2$	$(1.8 \pm 0.6) \times 10^2$
a [(GeV/c)$^{-1}$]	0.41 ± 0.22	0.42 ± 0.09
b [(GeV/c)$^{-2}$]	0.22 ± 0.16	0.20 ± 0.07
p_0 [GeV/c]	0.70 ± 0.09	0.69 ± 0.04
n	8.02 ± 0.15	8.01 ± 0.07

be expressed as

$$\mathrm{BG}^{\mathrm{SUM}}_{+-} = \alpha_{\mathrm{acc}}(\mathrm{FG}_{--} + \mathrm{FG}_{++}). \quad (6)$$

The acceptance-correction factor α_{acc} is calculated as the ratio of like- and unlike-sign pairs from mixed events.

Figure 4 shows the background pair distributions of e^+e^- determined by the like-sign subtraction technique and the method used here for p_T of 1–2 and 2−3 GeV/c, respectively. The two distributions are consistent within the statistical errors. The present method yields a smaller uncertainty, particularly at high p_T. The combinatorial background [dashed (red) curves] has a much more significant contribution in $\mathrm{BG}^{\mathrm{SUM}}$ compared with those of the cross pairs [dotted (blue) curves] and jet-induced correlations [dashed-dotted (green) curves].

5. Correlated pairs from hadron decays

The last e^+e^- background source (indicated as HD_{+-}) for the direct virtual photon signal is the known hadron decays. The invariant yields of π^0 in the 200 GeV Cu+Cu as measured by PHENIX [22] have been successfully parametrized by a modified Hagedorn fit:

$$E\frac{d^3\sigma}{dp^3} = A\left(e^{-(ap_T+bp_T^2)} + p_T/p_0\right)^{-n}. \quad (7)$$

The resulting Hagedorn fit parameters for 0%–40% and MB samples are listed in Table I.

Note that the large uncertainty of the absolute scale parameter A does not affect the direct-photon result because only the shape enters in determining the direct-photon fraction. A detailed description of this analysis appears in the next section, Sec. III B. m_T scaling of the parametrized π^0 yield has been shown to accurately reproduce the invariant yields of other known hadrons [11]. All known hadron decays producing e^+e^- are simulated with this parametrization by a Monte Carlo event generator within the PHENIX framework [15] and passed through the PHENIX GEANT3 simulation. The simulated e^+e^- pair mass distributions for known hadrons are merged as a "cocktail" of the hadron decay contributions. The particle compositions in the hadronic cocktail are based on the measured yields. The particle ratios to the π^0 yield are identical to the $p+p$ data [23].

An additional source of decay background is e^+e^- pairs from open heavy flavor decays. They hide behind the cocktail of photonic decays discussed previously in the mass region of interest below $m_{ee} = 0.3$ GeV/c^2. Their contribution becomes significant only around 0.6 GeV/c^2, and then dominant in the high-mass region above 1 GeV/c^2 because of their large opening angle. Their low mass contribution can be extrapolated by using a model fit to the data in the high-mass region [21]. PHENIX has reported that the low-mass distribution has a model dependence [16]. This model dependence results in a 100% uncertainty, particularly on the $c\bar{c}$ contribution. The open heavy flavor contribution is evaluated by binary scaling of the d+Au result [21]. However, the $c\bar{c}$ contribution is less than 0.1% at most in the mass region of interest, 0.3 GeV/c^2, even if 100% uncertainty from the model dependence is taken into account.

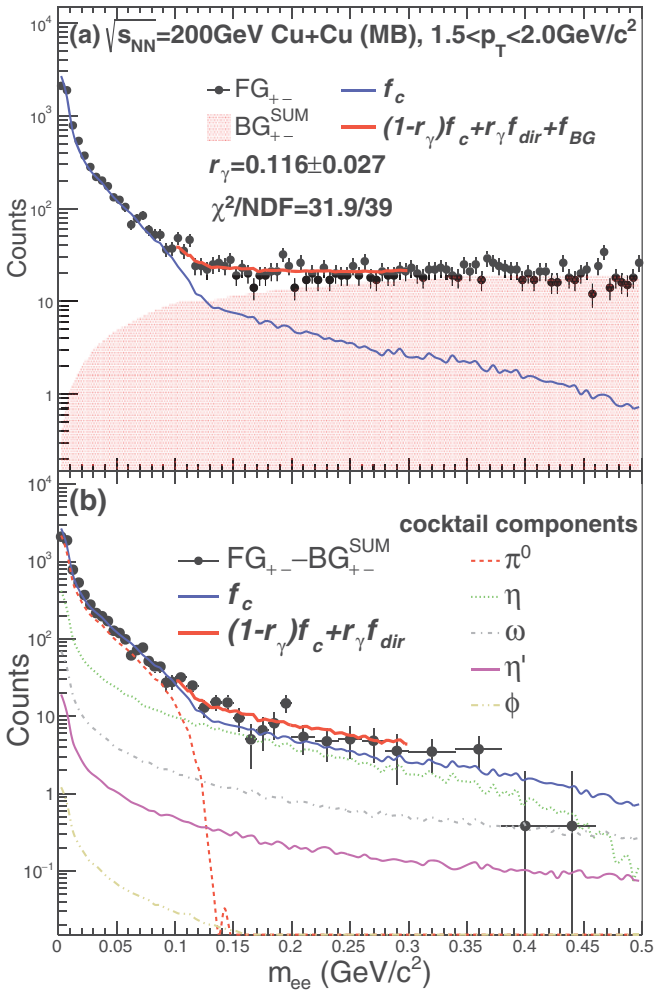

FIG. 5. The e^+e^- pair mass distribution in Cu+Cu MB collisions for $1.5 < p_T < 2.0$ GeV/c. (a) The data [closed (black) circles], fit to the data $(1 - r_\gamma) f_c + r_\gamma f_{\mathrm{dir}} + f_{\mathrm{BG}}$ [thick (red) curve], hadronic contribution [thin (blue) curve], and $\mathrm{BG}^{\mathrm{SUM}}_{+-}$ [shaded (red) region]. (b) The data after $\mathrm{BG}^{\mathrm{SUM}}_{+-}$ subtraction [closed (black) circles], the fit [thick (red) curve], hadronic contribution [thin (blue) curve], and cocktail components (indicated curves; see legend).

B. Determination of direct-photon fraction

The direct virtual photon signal is now extracted as the remainder of the signal above the backgrounds described in the previous section, Sec. III A. A similar fitting procedure to the one described in Ref. [6] is employed, in which Eq. (8) is fit to the mass distribution, with the following difference: In

the previous analysis only the hadronic cocktail was included in the fit. In the present measurement, the open heavy flavor and $\mathrm{BG}^{\mathrm{SUM}}$ contributions, which were subtracted before the fit in the previous measurements, are now included together with the hadronic cocktail as fixed contributions in the fit as Eq. (8). This is done in order for a log-likelihood fit to work properly even with limited statistics in the data, especially at higher p_T:

$$f(m_{ee}) = (1 - r_\gamma) f_c(m_{ee}) + r_\gamma f_{\mathrm{dir}}(m_{ee}) + f_{\mathrm{BG}}(m_{ee}), \quad (8)$$

where r_γ is the only fit parameter and f_c and f_{BG} are the hadronic cocktail and the fixed contribution of a sum of the open heavy flavor and $\mathrm{BG}^{\mathrm{SUM}}$ pairs, respectively. The expected mass shape of the direct virtual photons, f_{dir}, is calculated by a Monte Carlo simulation based on Eq. (1). It does not show the drop that appears in the mass shapes of e^+e^- pairs from π^0, η Dalitz decays because of $S \sim 1$ in Eq. (1). f_{dir}, f_c are normalized for $m_{ee} < 0.03\ \mathrm{GeV}/c^2$ before the fit to ensure that the fit result matches the data at $m_{ee} = 0$, where f_{dir} and f_c are identical. Finally, a log-likelihood fit is performed within a fit range of $0.1 < m_{ee} < 0.3\ \mathrm{GeV}/c^2$ to determine the direct virtual photon fraction for several p_T bins separately [$1 < p_T < 1.5$, $1.5 < p_T < 2.0$, $2.0 < p_T < 3.0$, $3.0 < p_T < 5.0\ \mathrm{GeV}/c$].

Figure 5 shows the e^+e^- pair mass distributions in Cu+Cu MB collisions for $1.5 < p_T < 2.0\ \mathrm{GeV}/c$. Figure 5(a) shows the data, the fit, the hadronic contribution, and the background $\mathrm{BG}^{\mathrm{SUM}}_{+-}$. Figure 5(b) shows the data and fit after $\mathrm{BG}^{\mathrm{SUM}}_{+-}$ subtraction, the hadronic contribution, and cocktail components.

C. Systematic uncertainties

The major sources of systematic uncertainties of the direct-photon fraction are

(1) the background normalization,
(2) the particle composition of the hadronic cocktail,
(3) the e^+e^- mass range for the log-likelihood fit.

To evaluate the uncertainty of the direct-photon fraction, the fraction is recalculated by using the same procedure and varying each source within $\pm 1\sigma$ of its uncertainty. The differences from the nominal value are quantified and taken as contributions to the uncertainty of the direct-photon fraction. An uncertainty of about 15%–40% comes from the fit mass range with different fit starting points from 0 to 0.15 GeV/c^2. The particle compositions, dominantly π^0/η add another 5%–15%. An additional 9.6% and 10% uncertainties are introduced from the MB trigger efficiency and e^+e^- pair acceptance when converting the direct-photon fraction to the yield. Total systematic uncertainties are calculated as a quadratic sum.

IV. RESULTS AND DISCUSSION

A. Direct-photon fraction

The direct-photon fraction as a function of p_T is obtained for two different centrality classes, MB and 0%–40%. Figure 6 shows the comparison of the direct-photon fraction r_γ, measured with the virtual photon method for different collision systems at $\sqrt{s_{NN}} = 200$ GeV from left to right: $p+p$ [9], d+Au (MB) [9], Cu+Cu (MB), and Au+Au (MB) [6].

The statistical and systematic uncertainties are shown together with the data points. Curves indicate the expectations

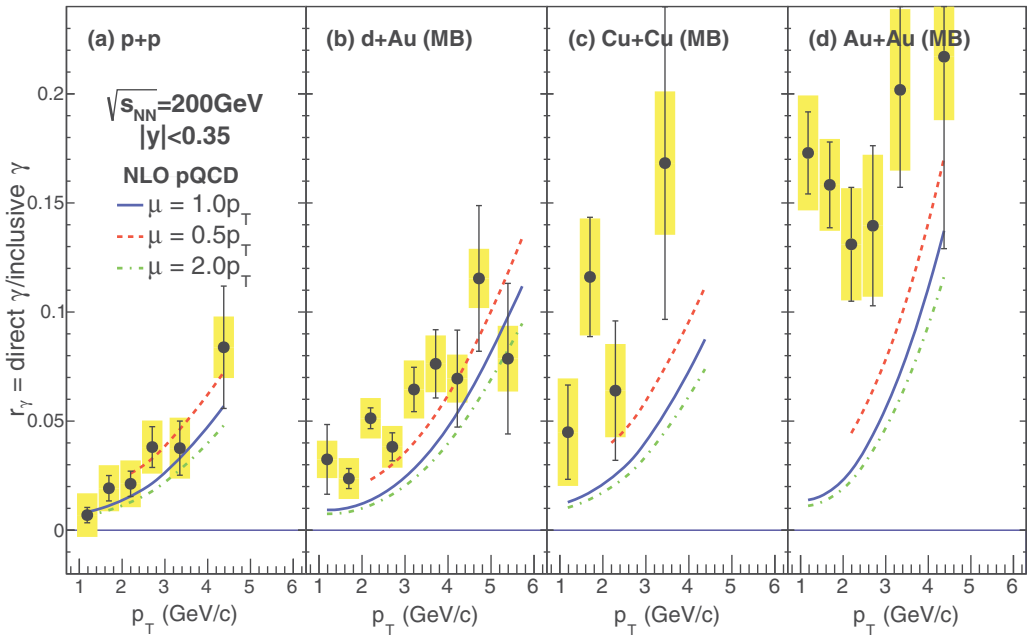

FIG. 6. Direct-photon fraction measured with the virtual photon method for different systems in $\sqrt{s_{NN}} = 200$ GeV collisions: (a) $p+p$ [9], (b) d+Au (MB) [9], (c) Cu+Cu (MB), (d) Au+Au (MB) [6]. Expectations from NLO pQCD calculations [24] are also shown by curves with different cutoff mass scales μ.

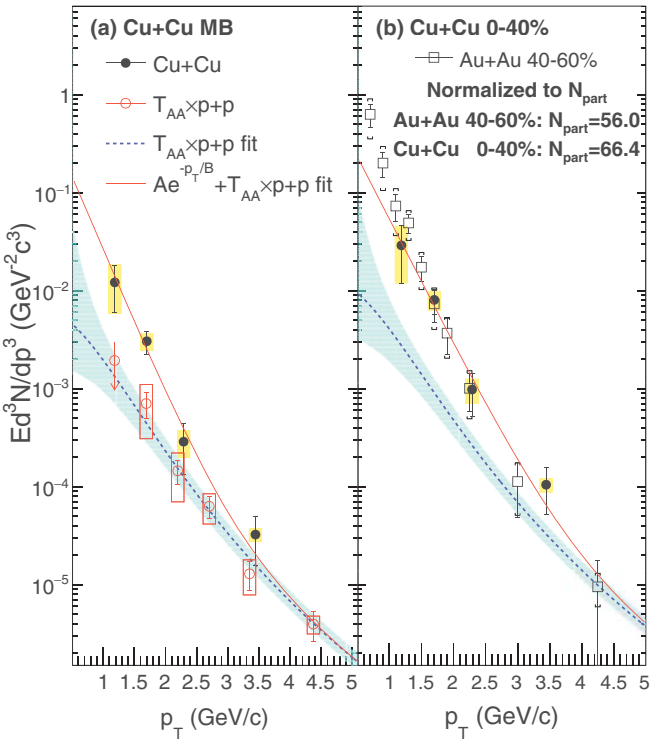

FIG. 7. The direct-photon spectra [closed (black) circles] for 200 GeV Cu+Cu (a) MB and (b) 0%–40% centralities. The T_{AA}-scaled $p+p$ data and fits together with uncertainties are shown as the open (red) circles symbols and the dotted (blue) curves and accompanying (red) boxes and (blue) bands. Au+Au 40%–60% centrality data points, which have a similar $N_{\rm part}$ as the Cu+Cu 0%–40% centrality data, are shown as the open (black) squares, where the Au+Au points are scaled by the $N_{\rm part}$ ratio (66.4/56.0). An exponential fit to the Cu+Cu data of the excess yield over the scaled $p+p$ fit [solid (red) curve] yields inverse slopes of $285 \pm 53(\text{stat}) \pm 57(\text{syst})$ MeV/c for MB and $333 \pm 72(\text{stat}) \pm 45(\text{syst})$ MeV/c for 0%–40%.

from a next-to-leading-order (NLO) perturbative-quantum-chromodynamics (pQCD) calculation [24] with different cut-off mass scales μ. While the $p+p$ and $d+$Au results show agreements with the NLO pQCD calculation, an excess over the NLO pQCD calculation is seen in the Cu+Cu data as well as in Au+Au. The Cu+Cu excess is rather modest compared with Au+Au, possibly due to a smaller volume of the created medium.

B. Direct-photon spectra

The obtained direct-photon fractions are converted to direct-photon yields by using the inclusive photon yields calculated by the same Monte Carlo simulation used for the e^+e^- pairs of the hadronic cocktail. Figure 7 shows the direct-photon spectra for Cu+Cu MB and 0%–40% most-central events. The $p+p$ results [9] parametrized by a modified power-law function $A_{pp}(1 + {p_T}^2/B_{pp})^{n_{pp}}$ and its $T_{\rm AA}$-scaled functions are shown as the dotted curves together with the data points. The modified power law is an empirical parametrization describing the $p+p$ result well, especially at low p_T.

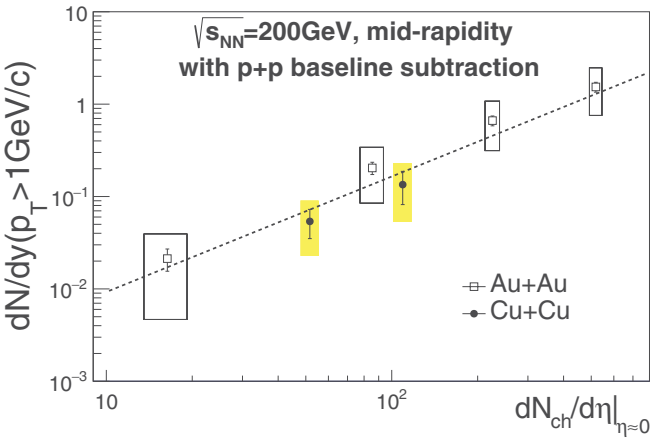

FIG. 8. Rapidity densities of the excess yield of direct photons over the scaled $p+p$ fits for $p_T > 1$ GeV/c at midrapidity as a function of $dN_{\rm ch}/d\eta$. The Au+Au data points with different centralities [7] and the power-law fit with the fixed power of 1.25 to both Cu+Cu and Au+Au data points are shown together.

The same function has been employed in previous low p_T direct-photon publications in heavy-ion collisions [6,7]. We have performed a least squares analysis in which p_T-correlated and p_T-uncorrelated errors are properly taken into account. A detail description of constraint parametrization can be found in Ref. [25]. The $p+p$ data points measured by the EMCal in $4 < p_T < 10$ GeV/c are included in the fit in addition to the virtual photon measurement covering $p_T < 6$ GeV/c. Here the lowest p_T data point is just an upper limit. The best fit gives $\chi^2/\text{NDF} = 18.9/17$, which is the minimum obtained by variation of the p_T-correlated errors. The uncertainty of the $p+p$ fit is calculated by using the error matrix of the fit parameters and is indicated as bands on the scaled $p+p$ fits. A different empirical parametrization, employed in Ref. [9], was tested as well. We treat the small deviation we find above 1 GeV/c as a maximum-extend error. We divide the deviation by $\sqrt{12}$ and add it in quadrature to the uncertainty of the fit.

An exponential fit to the excess yield above the scaled $p+p$ fits gives inverse slopes of $285 \pm 53(\text{stat}) \pm 57(\text{syst})$ MeV/c for MB and $333 \pm 72(\text{stat}) \pm 45(\text{syst})$ MeV/c for 0%–40% centrality. Furthermore, the Cu+Cu 0%–40% centrality result is compared with the Au+Au 40%–60% data scaled by the $N_{\rm part}$ ratio (66.4/56.0), which is consistent within uncertainties [see Fig. 7(b)].

C. Rapidity density

We further investigate the $N_{\rm part}$ dependence of the direct-photon yields as discussed in Ref. [7]. It has been reported that the Au+Au results [26] show an increasing trend for $N_{\rm part}$. The Cu+Cu data points help to have a closer look at the dependence in the small-$N_{\rm part}$ region. The rapidity density for $p_T > 1$ GeV/c at midrapidity, $dN/dy(p_T > 1\ \text{GeV}/c)$, is calculated by summing the direct-photon yields in given p_T

TABLE II. $dN_{\rm ch}/d\eta$, $N_{\rm coll}$, $N_{\rm part}$, the inverse slope of the exponential fits, and $dN/dy(p_T > 1\ {\rm GeV}/c)$ of the excess yield of direct photons over the scaled $p+p$ fits for 0%–40% and MB Cu+Cu collisions.

Centrality	$dN_{\rm ch}/d\eta$	$N_{\rm coll}$	$N_{\rm part}$	Inverse slope (MeV/c)	$dN/dy(p_T > 1\ {\rm GeV}/c)$
0%–40%	109.3 ± 7.8	108.2 ± 12.0	66.4 ± 2.5	$333 \pm 72 \pm 45$	$(1.3 \pm 0.5^{+0.9}_{-0.8}) \times 10^{-1}$
MB	51.7 ± 3.6	51.8 ± 5.6	34.6 ± 1.2	$285 \pm 53 \pm 57$	$(5.4 \pm 1.9^{+3.6}_{-3.1}) \times 10^{-2}$

bins taking the bin width correction into account:

$$\frac{dN}{dy} = 2\pi \sum_{p_T{}^i > 1{\rm GeV/c}} \left(p_T{}^i y_\gamma^i C_{bw}^i \Delta p_T{}^i\right), \tag{9}$$

$$C_{bw}^i = \int_{p_{T,\rm min}}^{p_{T,\rm max}} f_{\rm fit}(p_T) dp_T / [f_{\rm fit}(p_T{}^i)\Delta p_T{}^i], \tag{10}$$

where $p_T{}^i$, y_γ^i, and $\Delta p_T{}^i$ are the mean p_T, the direct-photon yield, and the p_T-bin width for the ith p_T bin. The bin-width correction C_{bw} is evaluated based on the fit function $f_{\rm fit}$ to the data shown in Fig. 7. C_{bw} contributes an additional 3.5% uncertainty of dN/dy. Then, dN/dy for the binary-scaled $p+p$ fit [26] is subtracted. Figure 8 shows dN/dy of the excess yield over the scaled $p+p$ fit as a function of measured charged multiplicity $dN_{\rm ch}/d\eta$ at midrapidity. A simple power-law fit with the fixed power of 1.25, $(dN_{\rm ch}/d\eta)^{1.25}$, is done for both the Cu+Cu and Au+Au results as done in Ref. [26]. It works very well to describe the $dN_{\rm ch}/d\eta$ dependence.

The inverse slope of the exponential fits and the rapidity density of the excess yield of direct photons over the scaled $p+p$ fits for $p_T > 1$ GeV/c are summarized together with $dN_{\rm ch}/d\eta$, $N_{\rm coll}$, $N_{\rm part}$ corresponding to 0%–40%, MB Cu+Cu collisions in Table II.

V. SUMMARY AND CONCLUSIONS

Low-p_T direct photons have been measured by using the virtual photon method for MB and 0%–40% most-central collisions in $\sqrt{s_{NN}} = 200$ GeV Cu+Cu collisions. A clear excess yield of direct photons over the binary-scaled $p+p$ baseline is seen for Cu+Cu as in the previously reported Au+Au results. The Cu+Cu direct-photon p_T spectra are consistent with the Au+Au data for similar $N_{\rm part}$. The exponential fits to the excess over the binary-scaled $p+p$ baseline give inverse slopes of $285 \pm 53({\rm stat}) \pm 57({\rm syst})$ MeV/c for MB and $333 \pm 72({\rm stat}) \pm 45({\rm syst})$ MeV/c for 0%–40% centrality. The Cu+Cu data points improve our knowledge of the system size dependence of the excess yield of the direct photons, especially in the small-$N_{\rm part}$ region. The Cu+Cu results on dN/dy for $p_T > 1$ GeV/c follow the same $dN_{\rm ch}/d\eta$ dependence as the Au+Au data as described by a simple power law.

ACKNOWLEDGMENTS

We thank the staff of the Collider-Accelerator and Physics Departments at Brookhaven National Laboratory and the staff of the other PHENIX participating institutions for their vital contributions. We acknowledge support from the Office of Nuclear Physics in the Office of Science of the Department of Energy, the National Science Foundation, Abilene Christian University Research Council, Research Foundation of SUNY, and Dean of the College of Arts and Sciences, Vanderbilt University (U.S.A), Ministry of Education, Culture, Sports, Science and Technology and the Japan Society for the Promotion of Science (Japan), Conselho Nacional de Desenvolvimento Científico e Tecnológico and Fundação de Amparo à Pesquisa do Estado de São Paulo (Brazil), Natural Science Foundation of China (People's Republic of China), Croatian Science Foundation and Ministry of Science and Education (Croatia), Ministry of Education, Youth and Sports (Czech Republic), Centre National de la Recherche Scientifique, Commissariat à l'Énergie Atomique, and Institut National de Physique Nucléaire et de Physique des Particules (France), Bundesministerium für Bildung und Forschung, Deutscher Akademischer Austausch Dienst, and Alexander von Humboldt Stiftung (Germany), J. Bolyai Research Scholarship, EFOP, the New National Excellence Program (ÚNKP), NKFIH, and OTKA (Hungary), Department of Atomic Energy and Department of Science and Technology (India), Israel Science Foundation (Israel), Basic Science Research and SRC(CENuM) Programs through NRF funded by the Ministry of Education and the Ministry of Science and ICT (Korea), Physics Department, Lahore University of Management Sciences (Pakistan), Ministry of Education and Science, Russian Academy of Sciences, Federal Agency of Atomic Energy (Russia), VR and Wallenberg Foundation (Sweden), the U.S. Civilian Research and Development Foundation for the Independent States of the Former Soviet Union, the Hungarian American Enterprise Scholarship Fund, the US-Hungarian Fulbright Foundation, and the US-Israel Binational Science Foundation.

[1] K. Adcox *et al.* (PHENIX Collaboration), Formation of dense partonic matter in relativistic nucleus-nucleus collisions at RHIC: Experimental evaluation by the PHENIX Collaboration, Nucl. Phys. A **757**, 184 (2005).

[2] J. Adams *et al.* (STAR Collaboration), Experimental and theoretical challenges in the search for the quark gluon plasma: The STAR Collaboration's critical assessment of the evidence from RHIC collisions, Nucl. Phys. A **757**, 102 (2005).

[3] G. David, R. Rapp, and Z. Xu, Electromagnetic Probes at RHIC-II, Phys. Rep. **462**, 176 (2008).

[4] P. Stankus, Direct photon production in relativistic heavy-ion collisions, Annu. Rev. Nucl. Part. Sci. **55**, 517 (2005).

[5] S. Turbide, R. Rapp, and C. Gale, Hadronic production of thermal photons, Phys. Rev. C **69**, 014903 (2004).

[6] A. Adare *et al.* (PHENIX Collaboration), Enhanced Production of Direct Photons in Au + Au Collisions at $\sqrt{s_{NN}} = 200$ GeV and Implications for the Initial Temperature, Phys. Rev. Lett. **104**, 132301 (2010).

[7] A. Adare *et al.* (PHENIX Collaboration), Centrality dependence of low-momentum direct-photon production in Au+Au collisions at $\sqrt{s_{NN}} = 200$ GeV, Phys. Rev. C **91**, 064904 (2015).

[8] L. Adamczyk *et al.* (STAR Collaboration), Direct virtual photon production in Au + Au collisions at $\sqrt{s_{NN}} = 200$ GeV, Phys. Lett. B **770**, 451 (2017).

[9] A. Adare *et al.* (PHENIX Collaboration), Direct photon production in d + Au collisions at $\sqrt{s_{NN}} = 200$ GeV, Phys. Rev. C **87**, 054907 (2013).

[10] J. Adam *et al.* (ALICE Collaboration), Direct photon production in Pb-Pb collisions at $\sqrt{s_{NN}} = 2.76$ TeV, Phys. Lett. B **754**, 235 (2016).

[11] A. Adare *et al.* (PHENIX Collaboration), System-size dependence of open-heavy-flavor production in nucleus-nucleus collisions at $\sqrt{s_{NN}} = 200$ GeV, Phys. Rev. C **90**, 034903 (2014).

[12] A. Adare *et al.* (PHENIX Collaboration), Transverse energy production and charged-particle multiplicity at midrapidity in various systems from $\sqrt{s_{NN}} = 7.7$ to 200 GeV, Phys. Rev. C **93**, 024901 (2016).

[13] K. Adcox *et al.* (PHENIX Collaboration), PHENIX detector overview, Nucl. Instrum. Methods Phys. Res., Sect. A **499**, 469 (2003).

[14] A. Adare *et al.* (PHENIX Collaboration), Search for dark photons from neutral meson decays in p+p and d+Au collisions at $\sqrt{s_{NN}} = 200$ GeV, Phys. Rev. C **91**, 031901 (2015).

[15] A. Adare *et al.* (PHENIX Collaboration), Detailed measurement of the e^+e^- pair continuum in p+p and Au+Au collisions at $\sqrt{s_{NN}} = 200$ GeV and implications for direct photon production, Phys. Rev. C **81**, 034911 (2010).

[16] A. Adare *et al.* (PHENIX Collaboration) Dielectron production in Au+Au collisions at $\sqrt{s_{NN}} = 200$ GeV, Phys. Rev. C **93**, 014904 (2016).

[17] T. Sjostrand, S. Mrenna, and P. Z. Skands, PYTHIA 6.4 Physics and Manual, J. High Energy Phys. 06 (2006) 026.

[18] T. Sjostrand, S. Mrenna, and P. Z. Skands, A Brief Introduction to PYTHIA 8.1, Comput. Phys. Commun. **178**, 852 (2008).

[19] H. L. Lai, J. Huston, S. Kuhlmann, J. Morfin, Fredrick I. Olness, J. F. Owens, J. Pumplin, and W. K. Tung (CTEQ Collaboration), Global QCD analysis of parton structure of the nucleon: CTEQ5 parton distributions, Eur. Phys. J. C **12**, 375 (2000).

[20] R. Brun, F. Bruyant, M. Maire, A. C. McPherson, and P. Zanarini, GEANT3 (1987).

[21] A. Adare *et al.* (PHENIX Collaboration), Measurements of e^+e^- pairs from open heavy flavor in p+p and d+A collisions at $\sqrt{s_{NN}} = 200$ GeV, Phys. Rev. C **96**, 024907 (2017).

[22] A. Adare *et al.* (PHENIX Collaboration), Onset of π^0 Suppression Studied in Cu + Cu Collisions at $\sqrt{s_{NN}} = 22.4$, 62.4, and 200 GeV, Phys. Rev. Lett. **101**, 162301 (2008).

[23] S. S. Adler *et al.* (PHENIX Collaboration), Common Suppression Pattern of η and π^0 Mesons at High Transverse Momentum in Au + Au Collisions at $\sqrt{s_{NN}} = 200$ GeV, Phys. Rev. Lett. **96**, 202301 (2006).

[24] L. E. Gordon and W. Vogelsang, Polarized and unpolarized prompt photon production beyond the leading order, Phys. Rev. D **48**, 3136 (1993).

[25] A. Adare *et al.* (PHENIX Collaboration), Quantitative constraints on the opacity of hot partonic matter from semi-inclusive single high transverse momentum pion suppression in Au {+} Au collisions at $\sqrt{s_{NN}} = 200$ GeV, Phys. Rev. C **77**, 064907 (2008).

[26] A. Adare *et al.* (PHENIX Collaboration), Beam-energy and centrality dependence of direct-photon emission from ultra-relativistic heavy-ion collisions, arXiv:1805.04084.